ANNUAL REVIEWS

Annual Review of Nuclear and Particle Science

The Hubble Tension and Early Dark Energy

Marc Kamionkowski[1] and Adam G. Riess[1,2]

[1]William H. Miller III Department of Physics and Astronomy, Johns Hopkins University, Baltimore, Maryland, USA; email: kamion@jhu.edu

[2]Space Telescope Science Institute, Baltimore, Maryland, USA

Annu. Rev. Nucl. Part. Sci. 2023. 73:153–80

First published as a Review in Advance on August 24, 2023

The *Annual Review of Nuclear and Particle Science* is online at nucl.annualreviews.org

https://doi.org/10.1146/annurev-nucl-111422-024107

Keywords

cosmology, early Universe, cosmic microwave background

Abstract

Over the past decade, the disparity between the value of the cosmic expansion rate determined directly from measurements of distance and redshift and that determined instead from the standard Lambda cold dark matter (ΛCDM) cosmological model, calibrated by measurements from the early Universe, has grown to a level of significance requiring a solution. Proposed systematic errors are not supported by the breadth of available data (and unknown errors are untestable by lack of definition). Simple theoretical explanations for this Hubble tension that are consistent with the majority of the data have been surprisingly hard to come by, but in recent years, attention has focused increasingly on models that alter the early or pre-recombination physics of ΛCDM as the most feasible. Here, we describe the nature of this tension and emphasize recent developments on the observational side. We then explain why early-Universe solutions are currently favored and the constraints that any such model must satisfy. We discuss one workable example, early dark energy, and describe how it can be tested with future measurements. Given an assortment of more extended recent reviews on specific aspects of the problem, the discussion is intended to be fairly general and understandable to a broad audience.

Contents

1. INTRODUCTION

In his *Chronology of Science & Discovery*, Isaac Asimov (1) identified Hubble's discovery of the cosmic expansion as one of the two defining events of twentieth-century science (along with the discovery of DNA structure). Interestingly enough, the value Hubble inferred for the expansion rate (the Hubble constant)—the ratio of the recessional velocity to distance for the galaxies he observed—turned out to be too high by an order of magnitude. Such a rate provided less than 2 billion years for the Universe to have grown to its present size—far lower than the age of the Earth. This first Hubble tension, defined here as any discrepancy between the locally measured and cosmologically inferred expansion rates, was resolved with the discovery of two generations of stars and a consequence of prior measurements intermingling the two.

Determination of the Hubble constant has been a central aim of cosmology ever since; measurements could differ by almost a factor of two as late as the early 1990s before reaching a celebrated result of $H_0 = 72 \pm 8$ km s^{-1} Mpc^{-1} (2), a 10% state-of-the-art precision by the new millennium, through use of the Hubble Space Telescope (HST) to resolve Cepheid variables in distant galaxies [later recalibrated to 74 ± 2 (3)]. Coupled with the theoretical expectation of $\Omega_m \sim 1$, the low expansion age implied by these measurements, still a few gigayears younger than the oldest stars, set off another Hubble tension until the discovery of cosmic acceleration amended the composition and recent expansion history and the age of the Universe grew comfortably higher.

Cosmology has, however, blossomed since then and now resembles high-energy physics experiments with its huge data sets, sophisticated analyses, careful attention to systematic errors, and a successful standard cosmological model—Lambda cold dark matter (ΛCDM)—with precisely determined parameters. Still, two decades into the new century, we find ourselves yet again with a third Hubble tension, which is smaller in scale than prior ones but highly significant—an $\sim$8% discrepancy with $\gtrsim 5\sigma$ confidence. Each past Hubble tension has taught us something

HST: Hubble Space Telescope

Cepheid: a yellow supergiant star pulsating in the fundamental (radial) mode whose light curve period strongly correlates to its mass and luminosity

Lambda cold dark matter (ΛCDM): the standard cosmological model, in which dark energy is taken to be a cosmological constant

more interesting than the value of a parameter, and a new tension provides an opportunity for discovery. Will this one (again) auger new astrophysics or fundamental physics?

The lower value $H_0 = 67.4 \pm 0.5$ km s^{-1} Mpc^{-1} (4) of the Hubble constant is anchored by measurements of angular temperature and polarization fluctuations in the cosmic microwave background (CMB) that calibrate free parameters in the ΛCDM cosmological model. Similar values are obtained from spatial fluctuations in the galaxy distribution (5, 6), whose physical scale is calibrated by the CMB—an approach called an inverse distance ladder. These data map the statistical properties of the distribution of mass to a spectrum of physical scales set by the ΛCDM cosmological model. Chief of these scales is the sound horizon: the distance a primordial fluctuation can travel at the sound speed in an expanding Universe before its size is frozen when the Universe becomes transparent at $z \sim 1{,}000$. The Hubble constant is one of six parameters that are optimized to find agreement between this model and the data. Absent the CMB, comparing primordial deuterium abundance with big bang nucleosynthesis (BBN) predicted by the cosmological model in the early Universe provides similar results, leading to the useful summary that the most precise but indirect measures of the Hubble constant derived from ΛCDM as calibrated in the pre-recombination or early Universe give values in the range of 67 to 68 km s^{-1} Mpc^{-1}.

A higher range of 70 to 75 km s^{-1} Mpc^{-1} covers essentially all precise (≤5%), recent late-Universe measurements of the Hubble constant determined locally or directly—inferred by comparing (as Hubble did) the recessional velocities and distances of galaxies. The leading approach in terms of community investment of HST time, and the most replicated, yields $H_0 = 73.0 \pm 1.0$ km s^{-1} Mpc^{-1} (7–9), near the middle of the range (**Figure 1**; see also figure 2 in Reference 10). Here, the galaxy distance is inferred from the apparent brightness of a standard

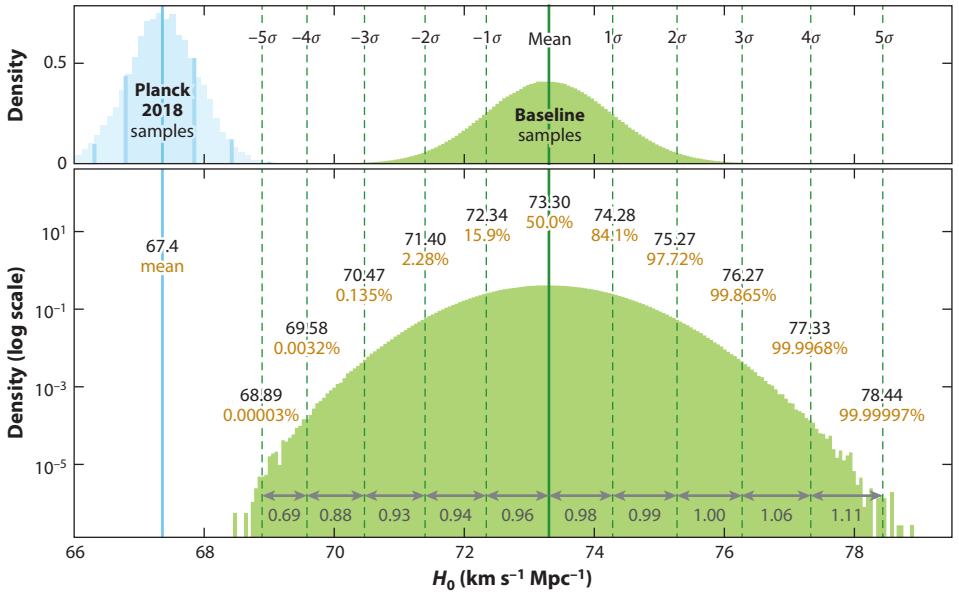

Figure 1

Extended Markov chain Monte Carlo sampling of the posterior for the Hubble constant H_0 to measure out to the 5σ confidence level. The top panel shows the probability density for the baseline from the Supernovae and H_0 for the Equation of State (SH0ES) Collaboration and from the Planck Collaboration chains (4). The bottom panel shows the log of the probability density to improve the ability to see the tails. Figure adapted from Reference 9 (CC BY 4.0).

candle (an astronomical source of fixed luminosity) or from the angular size of a standard rod (a source of calculable length). While Hubble used Cepheid variables (supergiant stars whose pulsation period correlates with their luminosity) as standard candles, current local measurements use a variety of standard candles and rods, but many rely on Type Ia supernovae (SNe Ia), a class of thermonuclear supernovae (stars with degenerate matter that approach the Chandrasekhar mass), to measure deep into the Hubble flow. We discuss uncertainties in the measurements in the next section.

Type Ia supernova (SN Ia): a supernova from thermonuclear detonation of a white dwarf when it exceeds the Chandrasekhar mass

The current Hubble tension has persisted while gaining in significance for nearly a decade, making it hard to ignore. Well-posed proposals of systematic errors in measurements have been tested and are not supported by the data, while nonspecific suggestions of measurement "unknown unknowns" are unsatisfactory and, by definition, untestable. A viable explanation is of interest not just to cosmology but also to physics. The standard cosmological model assembled in recent decades is remarkably successful, but it works only with ingredients that involve new physics beyond general relativity and the $SU(3) \times SU(2) \times U(1)$ Standard Model of elementary-particle physics. The Universe is observed on the largest distance scales to be quite smooth but with small density fluctuations well described as a realization of a Gaussian random field with a nearly scale-invariant power spectrum. The primordial origin of these perturbations, which have large correlation lengths, requires new physics (which can be very well described in the context of inflation) beyond the Standard Model. The time evolution of the perturbations in the baryons and in the photons visible to us as the CMB—as well as dynamics of galaxies and galaxy clusters in the Universe today—requires some form of collisionless dark matter that, again, requires new physics. Moreover, evidence for some negative-pressure dark energy (e.g., a cosmological constant) comes from supernova measurements (11, 12) and the detailed characterization of cosmological perturbations and also necessitates new physics.

Still, once collisionless dark matter, a cosmological constant, and a nearly scale-invariant spectrum of primordial perturbations are postulated, all of the data we have on the statistical properties of perturbations in the early and late Universe can be described by a model that is parameterized by (*a*) an overall amplitude for the primordial perturbation power spectrum, (*b*) a power law index for the power spectrum, (*c*) a baryon density, (*d*) a dark matter density, (*e*) the Hubble constant, and (*f*) a reionization optical depth that quantifies the fraction of CMB photons that are primordial.

While the Hubble tension looks prima facie to be a breakdown of ΛCDM's ability to connect two ends of cosmic time, it does not yield to easily anticipated, new-physics solutions. In considering the solution space, it is important to recognize that ΛCDM plays two distinct roles in the model-dependent calculation of H_0. First, the model is calibrated in its pre-recombination form ($z \gtrsim 1{,}000$) by comparison with primordial measurements to fix its six free parameters. Second, ΛCDM predicts the expansion history between $z \sim 1{,}000$ and $z \sim 0$, which leads to a prediction of H_0 with or without additional refinement of the model parameters that may come from comparison with low-redshift measures of the expansion history. A late-time solution affecting this extrapolation is attractive but appears less tractable. If the discrepancy were reversed—with a higher value for H_0 coming from the CMB—it could be easily attributed to the nature of dark energy as quintessence-like (13), where the dark energy density is slowly decreasing. However, such an explanation would require, given the larger H_0 from local measurements, that dark energy violate the dominant energy condition, something like a relativistic notion of creating energy from the vacuum. Even if we are willing to allow for such an exotic theoretical possibility, such a model is disfavored by galaxy clustering or high-redshift supernova measurements, which prefer a nearly constant Lambda-like dark energy density independent of the primordial measurements. Nor can the simplest dials on existing dark matter models be turned to solve the Hubble tension. Most analyses are done assuming a flat Universe, but allowing for some nonzero curvature

actually drives the CMB-inferred H_0 even lower. Workable solutions, and thus the ones we focus upon in this review, can be obtained by modifying ΛCDM at early times and its early cosmic-expansion history. One promising way is to postulate some sort of early dark energy (EDE) (14, 15) that behaves like a cosmological constant before matter–radiation equality but then decays away faster than radiation afterward. Recent CMB measurements made since EDE was proposed have improved sensitivity to polarization fluctuations on small angular scales and may even favor such models over ΛCDM. Still, we must await future CMB measurements and galaxy surveys to disprove either model.

A vigorous campaign to develop microphysical EDE models is now underway—at the time of submission of this article, there was about one new EDE model appearing every week. Most of them repurpose ideas explored earlier in connection with dark energy and/or inflation, but there are some novelties associated with the coincidence between the time that EDE becomes dynamical and the epoch of matter–radiation equality. Moreover, the machinery to produce precise model predictions is available, and so are the tools to make detailed comparisons with data sets. As a result, model building proceeds hand in hand with careful comparisons with ever-improving data. Some of the models suggest entirely new experimental/observational consequences of new EDE physics, which will hopefully bring new avenues to understanding the Hubble tension. There is also a slew of independent new techniques for local measurements that will further test the results of supernova measurements.

In this article, we review the Hubble tension and EDE at a colloquium level. There have been far too many developments in measurements and theory on this subject for us to review them in detail. Therefore, in our discussion of measurements we focus primarily on recent developments, current questions, and future prospects. The theory discussion emphasizes fundamental issues and model ingredients with relevant calculations presented schematically. We then describe the new-physics ingredients for a handful of EDE models.

Fortunately, there are excellent recent and broad reviews on various aspects of the Hubble tension (16–21) and the various types of models that have been invoked to explain it (19, 22). Some recent reviews on (late-time) dark energy (13, 23, 24) also cover some overlapping issues in theory and cosmological parameter determination.

2. OBSERVATIONS AND MEASUREMENTS

2.1. Defining the Hubble Constant

The Hubble constant H_0 is defined as the constant of proportionality in the relation $cz = H_0 D$ between distance D and redshift z in the limit $z \to 0$. For measurements that necessarily involve sources at $z > 0$, the linear relation is generalized to

$$D = \frac{cz}{H_0}\left\{1 - \left[1 + \frac{q_0}{2}\right]z + \left[1 + q_0 + \frac{q_0^2}{2} - \frac{j_0}{6}\right]z^2 + O(z^3)\right\},$$

which follows from a Taylor expansion of the scale factor

$$a(t) = a_0\left\{1 + H_0\,(t - t_0) - \frac{1}{2}\,q_0\,H_0^2\,(t - t_0)^2 + \frac{1}{3!}\,j_0\,H_0^3\,(t - t_0)^3 + O([t - t_0]^4)\right\},$$

with $H(t) = +(da/dt)/a$ as the expansion rate at time t, $q(t) = -(d^2a/dt^2)[H(t)]^{-2}/a$ as the deceleration parameter, $j(t) = (d^3a/dt^3)[H(t)]^{-3}/a$ as the jerk parameter, and so on. For simplicity these relations are defined without curvature, but they can be generalized with curvature. The Hubble

"constant" is then the expansion rate $H_0 = H(t_0)$ today (time t_0). We can determine H_0 (and q_0, j_0, etc.) from measurements of distances and redshifts directly from this definition and independent of the cosmological model.

Redshifts are easily measured from the change in wavelength of observed atomic transitions (usually emission lines of galaxies) compared with experimental laboratory values. Relative (also called uncalibrated or scale-free) distance measurements at $D > 100$ Mpc, where the ~200–300 km s^{-1} peculiar velocities (random velocities relative to the Hubble flow) become negligible, are readily obtained from the brightness of SNe Ia, which provide for determination of q_0 and j_0, while H_0 drops out of the calculation (25). The parameters q_0 and j_0 can also be constrained from other cosmological data. In either case, the uncertainties in local determinations of H_0 from uncertainties in q_0 and j_0 are irrelevantly small; a change Δq_0 changes H_0 by $O(\Delta q_0)$ in kilometers per second per megaparsec. Measurement of H_0 then requires absolute distance measurements; these must ultimately be calibrated by geometry and are harder to come by.

SH0ES: Supernovae and H_0 for the Equation of State

WFC3: Wide Field Camera 3

UVIS/IR: ultraviolet-visible/infrared, the two channels on WFC3 (UVIS = 200–1,000 nm; IR = 800–1,700 nm)

2.2. The Local Distance Ladder: Geometry to Cepheids to Type Ia Supernovae

For reasons related to the homogeneity and luminosity of different classes of astronomical objects, the most widely supported route for measuring H_0 has been to construct a three-step distance ladder using geometry to calibrate Cepheid variables followed by SNe Ia. Here we make reference to the specific implementation and most recent iteration of this approach by the Supernovae and H_0 for the Equation of State (SH0ES) team (9).

Cepheids have been favored as primary distance indicators for more than a century because they are very luminous (100,000 solar luminosities), extremely precise [3% in distance per source (26)], easy to identify due to their periodicity [since Leavitt & Pickering (27)], and well understood [since Eddington (28)]. They are massive, pulsating supergiant stars that overshoot hydrostatic equilibrium due to the κ temperature-dependent opacity mechanism (29). There is a tight coupling between the period of the pulsation (weeks to months), the mass, and the luminosity of these stars, with the luminosity inferred empirically from the period from Cepheids at a common distance. They are also the most consistently calibrated standard candle, an important issue for reduction of errors, thanks to the use of a single, stable telescope and instrument, the HST Wide Field Camera 3 (WFC3) ultraviolet-visible/infrared (UVIS/IR), for all measurements in local SN Ia hosts and in three geometric calibrators of Cepheid luminosities: the megamaser host NGC 4258 (30), Milky Way parallaxes from the ESA Gaia mission (31), and the Large Magellanic Cloud (26) (via detached eclipsing binaries) with a precision of 1.5%, 1.0%, and 1.2%, respectively. Milky Way parallaxes, from the Gaia mission in particular and through successive iterations, have become the best source of geometric distance measurements, moving the calibration of Cepheids ahead of other stellar distance indicators and even allowing for additional self-calibration of Gaia parallax errors (32). Near-infrared (NIR) observations of Cepheids are used to mitigate the impact of uncertainties related to dust and thereby reduce systematic uncertainties relative to past, optical-only data. Just recently, a serendipitous early James Webb Space Telescope (JWST) observation of NGC 1365, a nearby galaxy on the Cepheid–supernova calibration path, allowed a measurement of the NIR Cepheid period–luminosity relation with JWST's improved resolution (33). The results are consistent with HST's but show that future JWST observations will be an important tool in the increasingly precise characterization of Cepheids.

SNe Ia are rarer than Cepheids (one per galaxy per century versus hundreds per galaxy at any time)—hence, none have been near enough for a parallax measurement in 400 years—but they are far more luminous (billions of solar luminosities). Standardizable to 6% in distance per source, they have no rival in their ability to witness cosmic expansion. In the past, the uncertainty

in H_0 was limited by the rarity of SNe Ia whose hosts were in the range of Cepheids (at $D \leq 40$ Mpc—about one per year), but better instruments on HST and persistence have produced a complete sample of 42 well-observed, prototypical SNe Ia from the last four decades (the era of digital photometry). (The redshifts of these nearby SN Ia hosts do not enter the calculation of H_0.) Great efforts have been made to calibrate and standardize these consistently with the thousands of SNe Ia in the Hubble flow (25, 34) (typically at $0.02 < z < 0.15$), including the modeling of data covariance. The result is a measurement from the SH0ES and Pantheon+ data of $H_0 = 73.04 \pm 1.04$ km s^{-1} Mpc^{-1} including systematic uncertainties (see **Figure 2**).

This result has passed a wide range of null tests, it has been replicated from the published Cepheid photometry (35, 36), and the Cepheid photometry has been replicated independently (37). Sixty-seven variants of the baseline analysis (see **Figure 3**) demonstrate that it is difficult to move the central value below ∼72.5 or above ∼73.5 (for a discussion of uncertainties, see Reference 32). The relation between Cepheid metallicity and luminosity, a past source of uncertainty, has been well calibrated (38) and, because of the breadth of anchors, has little effect on H_0 in any case. Well-posed, experimental challenges to these measurements have been extensively studied and are certain to continue, but the present evidence does not support a significant challenge to the conclusions of a highly significant tension. The comparison to Planck with ΛCDM yields the strongest evidence for the Hubble tension at 5σ, or 5.3σ when including new calibrations from Gaia clusters (39).

Nevertheless, it is important to test the individual rungs of this ladder. Testing can be done with other independent distance indicators, such as surface-brightness fluctuations (SBFs), tip of the red-giant branch (TRGB), type II supernovae (SNe II), and Miras (see figure 2 in Reference 10, which presents a composite view of a large sample of local-measurement results). For reference, to calibrate the nearest SN Ia, a distance indicator needs to reach galaxies at $D > 10$ Mpc. To well calibrate the Hubble flow, a distance indicator needs to reach $D \sim 100$ Mpc, so that $O(1{,}000$ km s$^{-1})$ peculiar velocities are small compared with the Hubble-flow velocity. To be calibrated by parallax, the distance indicator needs to be present in the Milky Way.

SBF: surface-brightness fluctuation

TRGB: tip of the red-giant branch

Type II supernova (SN II): a core-collapse supernova distinguished by hydrogen in its spectrum

AGB: asymptotic-giant branch (like a red giant, but having burned its helium core to carbon or heavier elements)

2.3. Other Local Measurements

2.3.1. Tip of the red-giant branch. When a main-sequence star has burned all the hydrogen in its core to helium, the star continues to burn hydrogen in a shell around the core, thus slowly increasing the helium-core mass. During this time, the star becomes cooler but brighter, a process that continues until the mass, and thus temperature, of the helium core becomes large enough (about 0.5 solar masses) to ignite helium burning to carbon. The luminosity of the I-band (in the infrared) is seen to be insensitive to the star's metallicity and mass, and so it can be used as a standard candle. Since the TRGB luminosity is 10 times fainter than long-period Cepheids, it is more limited in distance to $D < 20$ Mpc. It has, however, been used in lieu of Cepheid variables to calibrate nearby SNe Ia.

In practice, the location of the tip in the color–magnitude diagram of stars often appears fuzzy because of the presence of asymptotic-giant branch (AGB) stars, which have the same color as red-giant branch stars but are both brighter and fainter, reducing the contrast and blurring the location of the tip (for an illustration of the TRGB measurement process, see **Figure 4**). Varying degrees of contamination of the old, metal-poor halo tip by new star formation or crowding may be partially mitigated by careful selection of regions to analyze (40) while leaving some ambiguity about the location of the tip, which is field dependent. Techniques to measure the tip include Sobel edge detection, parametric luminosity function fitting, and maximum likelihood methods. TRGB, like Cepheids, is not generally used to measure H_0 directly, but it contributes to such measurements by calibrating longer range indicators.

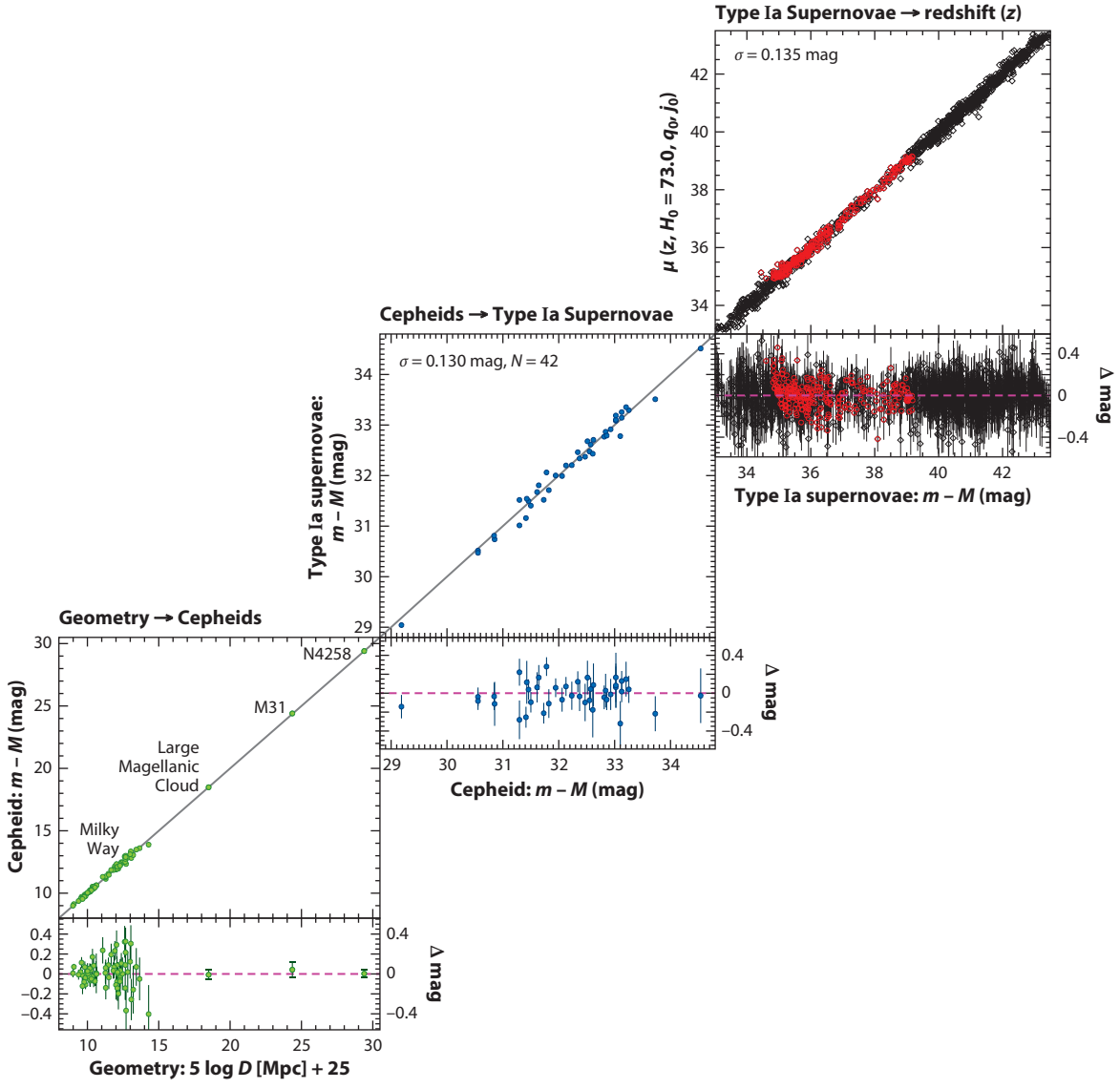

Figure 2

The cosmic distance ladder used by the Supernovae and H_0 for the Equation of State (SH0ES) Collaboration to infer the Hubble constant H_0. The luminosities of nearby Cepheid variables are calibrated to parallaxes. Supernova luminosities are then calibrated to Cepheid luminosities at larger distances. The Hubble constant is then inferred from the brightnesses of more distant supernovae. Figure adapted from Reference 9 (CC BY 4.0).

A direct comparison of Cepheids and TRGB and distance measures can be made in seven SN Ia hosts (both deriving calibration from the same geometric distance measure in NGC 4258), and these yield agreement to better than 2% in the mean (32). However, literature differences in the determination of H_0 involving TRGB are seen to arise from the other two rungs: the (first) calibration rung and a (third) SN Ia rung. There are several measures of H_0 that use TRGB including the Chicago-Carnegie Hubble Program (CCHP) (70 ± 2) (41); the Extragalactic Distance

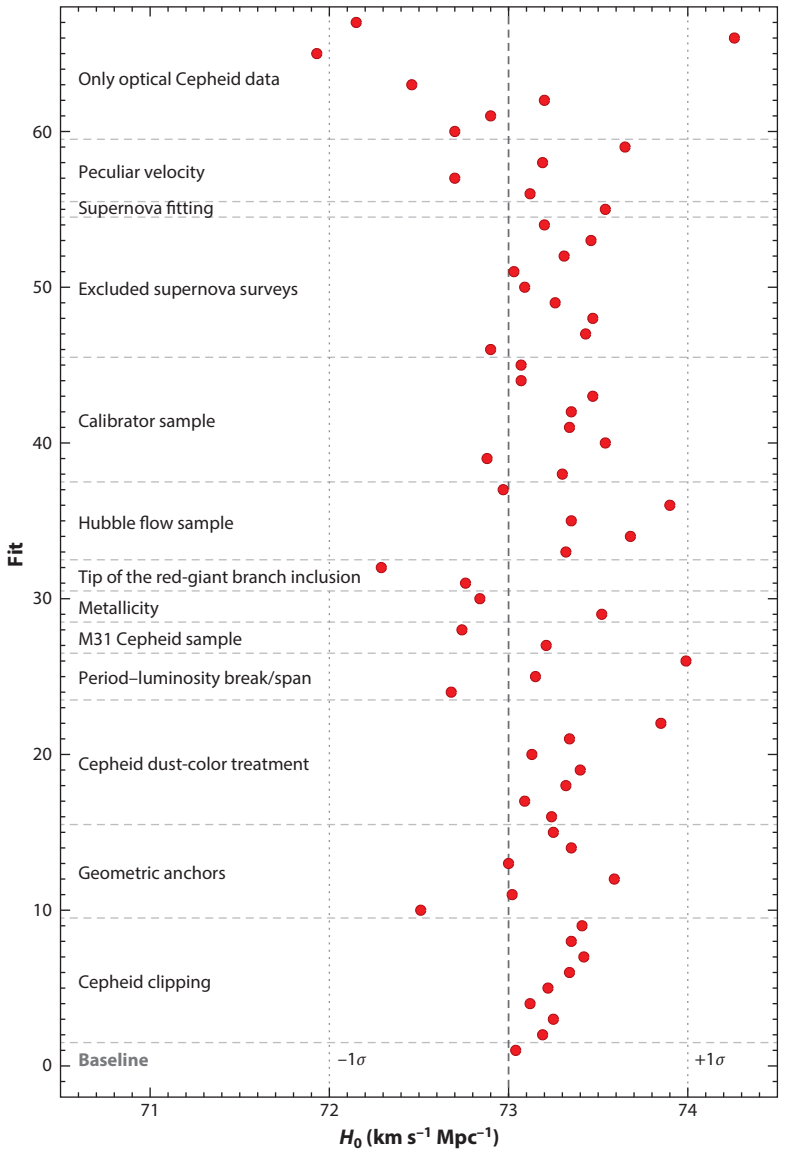

Figure 3

Values of the Hubble constant H_0 inferred by the Supernovae and H_0 for the Equation of State (SH0ES) Collaboration under different assumptions and analyses. The $\pm 1\sigma$ vertical dotted lines indicate the statistical error in the baseline result shown at the bottom. Figure adapted from Reference 9 (CC BY 4.0).

Database (EDD) (71.5 ± 2.0) (42), which connects to SNe Ia; and a measure that calibrates SBFs with TRGB (73 ± 3) (43). The main source of differences in the CCHP and EDD TRGB studies is in the determination of the TRGB in NGC 4258, which differs by 1.5 km s^{-1} Mpc^{-1} (in H_0). These groups use different fields in NGC 4258, and more work may elucidate how these fields compare to those used to measure TRGB around SN Ia hosts. Parallaxes from Gaia of field stars (44) or the nearby, massive globular cluster Omega Centauri (45) may also aid TRGB calibration

CCHP: Chicago-Carnegie Hubble Program

EDD: Extragalactic Distance Database

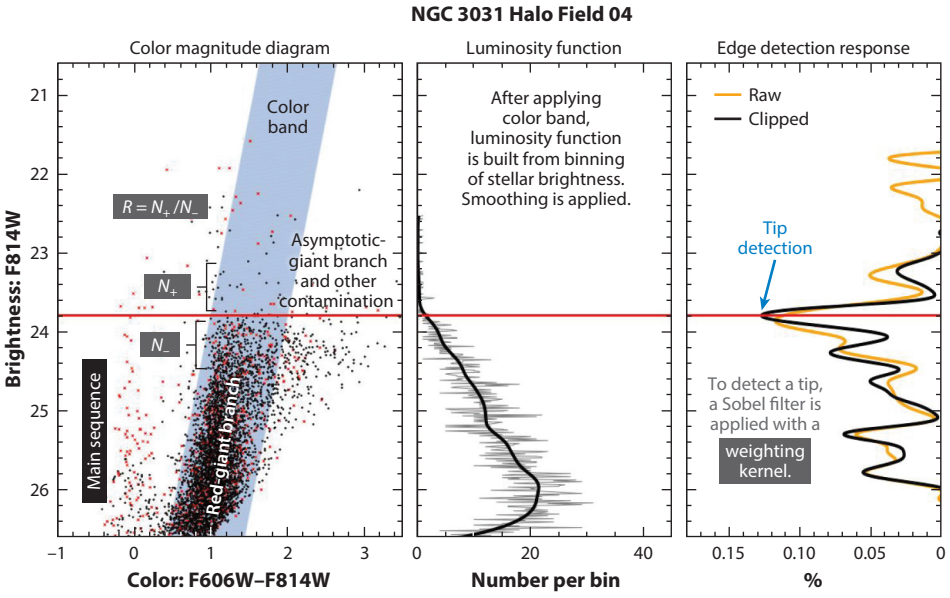

Figure 4

Steps involved in the inference of distances from the tip of the red-giant branch and some of the metrics used to judge the quality of the result. The tip contrast R is the most important of these. Figure adapted from Reference 151.

(for a summary of recent TRGB calibrations, see figure 6 in Reference 44). The lower value of H_0 from the CCHP study also partially stems from differences in its measurement of the Hubble flow from SNe Ia; accounting for local peculiar motions (46) and cross-calibration of supernova samples (47) would raise that H_0 by ∼1.5 km s^{-1} Mpc^{-1} (or likewise, we find that removing these steps in the SH0ES team measurement lowers that measurement to 71.8 km s^{-1} Mpc^{-1}). These are small differences that are important to understand to reach a 1% uncertainty. However, as seen in figure 2 of Reference 10, all local measures at this precision level are above the 67.4 ± 0.5 km s^{-1} Mpc^{-1} expectation (Planck), while none of the local measures are in tension with each other (at $>1.5\sigma$). Even the lowest value of these measures is above the 4σ confidence level of Planck.

2.3.2. Gravitational waves. The gravitational-wave (GW) signal from a merging neutron star binary can be used to determine the Hubble parameter (48). The spin-down frequency and GW amplitude can be used to determine the distance to the source as long as the inclination of the binary is known. The inclination can in principle be constrained with knowledge of the GW polarization. Even without polarization, the distribution of inclination angles can be averaged over multiple events. This measurement requires, however, a redshift obtained from an electromagnetic counterpart.

This technique was implemented with the detection (49–51) of a GW signal consistent with a neutron star–neutron star or neutron star–black hole merger at a distance ∼40 Mpc, as well as detection of an associated soft γ-ray burst and a slew of subsequent electromagnetic observations. This event, GW170817, then provided a measurement $H_0 = 74^{+16}_{-8}$ km s^{-1} Mpc^{-1} (68% confidence level) of the Hubble parameter (52), but the associated uncertainties—dominated by that for the inclination angle—were too large to be of value. Subsequent detection and modeling of a

late-time radio jet from the merger then constrained the inclination angle and thus improved the measurement to $H_0 = 70.3^{+5.3}_{-5.0}$ km s^{-1} Mpc^{-1}. The error reduction is, however, accompanied possibly by radio-jet modeling uncertainties. In addition, this event at $D \sim 40$ Mpc ($z \sim 0.01$) was too close to provide a clean measure of the Hubble flow; peculiar velocities produced an 8% uncertainty. Given the expected increase over the next decade in detection range, as well as improved characterization from multiple observatories, a robust $\lesssim$2% GW measurement of the Hubble parameter may be possible in the coming decade.

It may also be possible to constrain H_0 from GW events without optical counterparts. The idea of this so-called statistical siren or dark siren approach is that if the origin of the GW signal can be localized on the sky, then a catalog of candidate host galaxies can be obtained. Although H_0 cannot be determined from this method, the redshift distribution of the candidate hosts translates to a probability distribution for H_0 (53). By combining results from a large number of such events, the possible values of H_0 can be narrowed. The Laser Interferometric Gravitational-Wave Observatory (LIGO)/Virgo and Dark Energy Survey (DES) Collaborations (54) have applied this technique to GW170814, a particularly bright and reasonably well-localized event, although the H_0 constraints from this initial foray are not yet significant.

LIGO: Laser Interferometric Gravitational-Wave Observatory

Virgo: an interferometer managed by the European Gravitational Observatory

DES: Dark Energy Survey

2.3.3. Mira variables. Mira variables are pulsating, low-mass, intermediate-age (AGB) stars with great luminosity and are comparable to Cepheids in the NIR. The oxygen-rich subtype has a simple, linear period–luminosity relation. However, these objects are more challenging to find and measure than Cepheids because their periods are far longer (hundreds to a thousand days), and there are contaminating stars in the same period range (carbon-rich Miras and long-period variables) that must be distinguished using light-curve amplitudes and colors. First attempts to use Miras to supplant Cepheids or TRGB are promising (55), but the sample size is small.

2.3.4. Surface-brightness fluctuations. The SBF technique determines distances to galaxies by the SBFs that arise from the finite number of stars in the galaxy (56). The electromagnetic energy flux F from a given galaxy is related to its distance D by $F \propto D^2$, and the surface brightness is proportional to D^{-2}. If the galaxy is resolved, then there will be pixel-to-pixel variations in the surface brightness, induced by the finite number of stars contributing to the flux in any given pixel, with root variance proportional to D^{-1}. This technique yields distances with precision approaching that of SNe Ia but cannot reach the same distances. Nevertheless, SBFs offer an important alternative to SNe Ia, and a recent, state-of-the-art study of SBFs using HST in the NIR (43, 57) yields similar results as SNe Ia: $H_0 \sim 73.3 \pm 2.5$, whether calibrated by Cepheids or TRGB.

2.3.5. Masers. Water masers in Keplerian motion around supermassive black holes in the centers of galaxies can be observed in the radio using very long baseline interferometry (VLBI). By tracking proper motions and accelerations, a purely geometric distance can be measured to the maser host. However, such objects are rare given the requirement of edge-on alignment of the inner accretion disk with the observer's line of sight coupled with the need for an optimal density profile of the disk. The Megamaser Cosmology Project (MCP) measured six such systems in the Hubble flow and obtained $H_0 = 74 \pm 3$ (30), which was independent of any previously reviewed rungs. While this approach is limited in precision given the small samples and limited resolution of the galaxy nucleus, future observations of these same maser hosts with the Event Horizon Telescope (**https://eventhorizontelescope.org**) could yield a dramatic improvement and are highly anticipated.

2.4. Model-Dependent Local Measurements

wCDM: the cosmological model with dark energy with an equation-of-state parameter w

We now review several additional techniques to determine the Hubble constant that we refer to as model dependent because they require additional modeling: For gravitational lensing, it is a model for the lens mass; for ages and aging, it is a model for stellar evolution.

2.4.1. Strong gravitational lensing. If a given time-varying cosmological source is multiply lensed by a massive foreground object, there will be time delays between the light curves observed in the different images. These time delays depend on the angular diameter distances to the lens and source, thus providing a route to determine H_0 (58). Quasars have proved to be ideal targets for this measurement as they are bright, time-variable, and long-lived (59–62). In 2019, the H_0 Lenses in Cosmograil's Wellspring (H0liCOW) Collaboration reported $H_0 = 73.3^{+1.7}_{-1.8}$ km s^{-1} Mpc^{-1} from an analysis of six strongly lensed quasars with time delays (63). One issue in the measurement is the mass-sheet degeneracy (64): A flat mass distribution in the plane along the line of sight can add to the time delay without affecting the image locations and brightnesses. In practice, the mass distribution of the lens must be constrained with dynamical constraints to the lens mass, thus introducing new uncertain astrophysics into the measurement. As an illustration of the possible impact, a subsequent analysis of the H0liCOW quasars (with a seventh added) relaxing the assumption of a conventional galaxy mass profile for the lenses (Navarro–Frenk–White or power law) in one of two different ways obtained values consistent with either end of the H_0 discrepancy and with larger error bars (65). So if lenses share the same mass profiles as local, well-studied elliptical galaxies, lensing conforms with the other local values, and if it does not, the way in which it does not becomes the leading source of uncertainty. The strong-lensing determination of H_0 is now being advanced by the Time Delay Cosmography (TDCOSMO) Collaboration (66) with new systems, new analysis pipelines, and careful attention to identification and mitigation of systematic effects and astrophysical uncertainties.

2.4.2. Ages and aging. The expansion rate $H(z)$ at any given redshift z is inversely proportional to the ratio of the time interval Δt associated with some given redshift interval Δz. Reference 67 thus proposes using differential stellar ages to determine the expansion history and, at low redshifts, the Hubble parameter H_0. This type of measurement currently is most precise at a redshift $z \simeq 0.45$ (68, 69). This measurement is subject to stellar astrophysics uncertainties that have only recently been well studied (70, 71). Folding these in constrains H_0 to $67.8^{+8.7}_{-7.2}$ and 66.5 ± 5.4 km s^{-1} Mpc^{-1}, respectively, for a generic open wCDM and for a flat ΛCDM cosmology—results that are not very constraining in the present landscape.

The age of the Universe also provides a constraint to H_0. In a wCDM cosmology with matter density Ω_m and dark energy equation-of-state parameter w, it is

$$t_0 = \frac{1}{H_0} \int_0^\infty \frac{dz}{(1+z)\sqrt{\Omega_m (1+z)^3 + (1-\Omega_m)^{-3(1+w)}}}. \quad 1.$$

The oldest (observable) stars in the Universe are found in low-metallicity (thus formed from nearly primordial gas) globular clusters in the Milky Way halo. The stars in these globular clusters have nearly uniform metallicities and exhibit a clear main sequence in their color–magnitude diagrams, thus suggesting a uniform burst of star formation. The age is determined by fitting main-sequence isochrones from stellar evolution models to the observed color–magnitude diagram, as the main sequence is the best-understood phase of stellar evolution. Recent parallaxes from Gaia have reduced the uncertainties in the stellar luminosity and thus in the inferred ages. Using ages from 22 Milky Way globular clusters (72), Reference 73 obtains a value of $H_0 = 71.0 \pm 2.7$ km s^{-1} Mpc^{-1}. This provides a distance-ladder-independent measurement

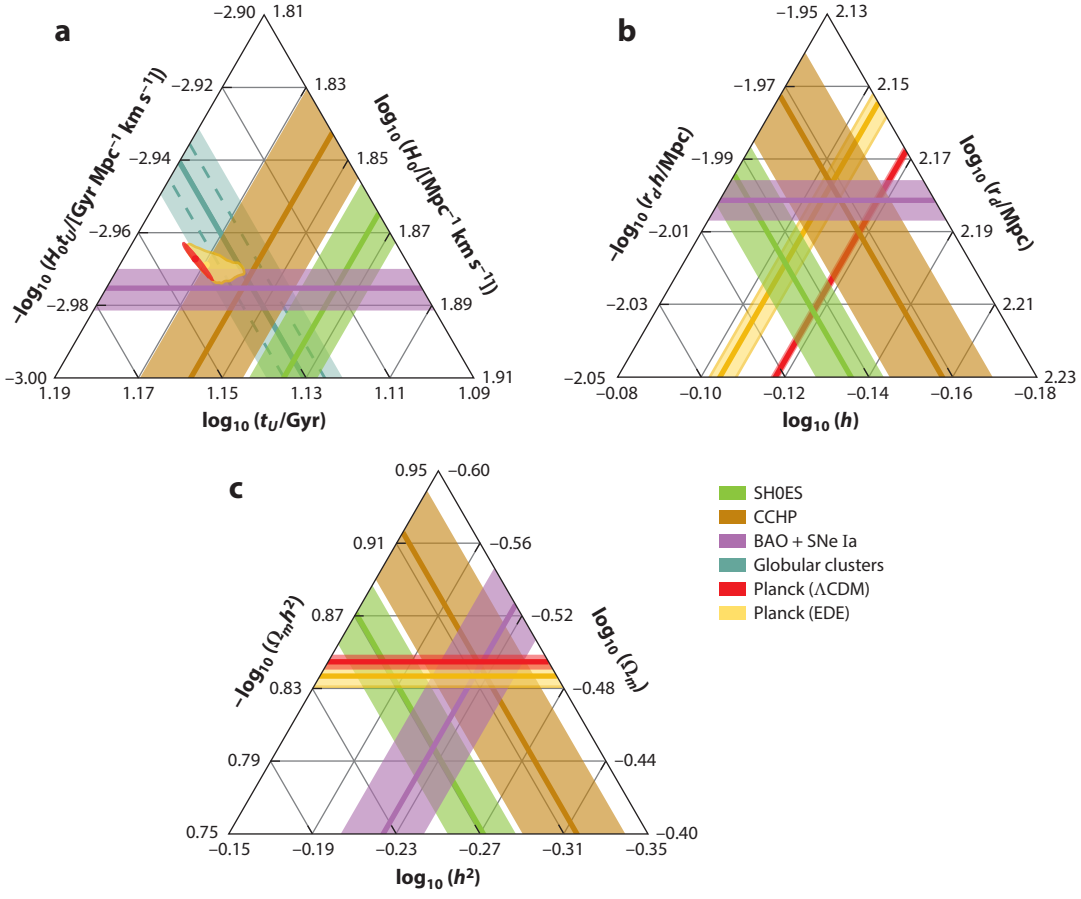

Figure 5

The 1σ allowed parameter regions in triads corresponding to (*a*) the age of the Universe and the Hubble constant, (*b*) the sound horizon at radiation drag and the reduced Hubble constant, and (*c*) the total matter density and the square of the reduced Hubble constant. Note that all points in each panel sum to zero, while the ticks in the axes determine the direction of equal values for each axis. Abbreviations: BAO, baryon acoustic oscillation; CCHP, Chicago-Carnegie Hubble Program; EDE, early dark energy; ΛCDM, Lambda cold dark matter; SH0ES, Supernovae and H_0 for the Equation of State; SN Ia, Type Ia supernova. Figure adapted from Reference 74.

and thus complements other H_0 determinations. The degeneracies with other cosmological parameters also complement those of CMB and local measurements, as shown in **Figure 5** (74).

3. EARLY-UNIVERSE MEASURES

3.1. The Sound Horizon, the Cosmic Microwave Background, and Large Scale Structure

The density of the early Universe (here, early means within the first ∼400,000 years of the Universe, before the CMB photons last scattered) was the same to $\lesssim 10^{-5}$ everywhere. It consisted of photons, baryons (∼75% protons by weight, ∼25% alpha particles, and electrons), all three neutrino mass eigenstates, and dark matter. The cosmological constant (or other form of dark energy) was dynamically insignificant. Efficient electron–photon scattering implies that the photons and baryons comprised one tightly coupled baryon–photon fluid. The neutrinos were noninteracting

(from a few seconds after the big bang) but had a thermal velocity distribution with a temperature ∼0.7 times the photon temperature. The dark matter is assumed to be entirely collisionless, an assumption verified by increasingly constraining null searches for dark matter interactions with baryons, photons, neutrinos, or itself.

The primordial Universe was also populated by adiabatic density perturbations well described as a realization of a Gaussian random field with power spectrum $P(k) \propto k^{n_s}$ as a function of wavenumber k. Here, adiabatic implies that the fractional density perturbation in each species was equivalent; that is, the baryon:photon:dark matter:neutrino ratio was the same everywhere. The scalar spectral index n_s is determined empirically to be $n_s \simeq 0.96$. The characteristics of this density field (i.e., n_s is close to, but not precisely equal to, unity; the adiabaticity; and Gaussianity) are all consistent with the simplest single-field slow-roll models of inflation. The details of inflation (or even whether it ever occurred) are not relevant to the Hubble tension; we can simply take the flat Universe and nearly scale-invariant spectrum of adiabatic perturbations as empirical facts.

3.1.1. The sound horizon in the baryon–photon fluid and baryon acoustic oscillations. Consider a Dirac delta function adiabatic overdensity of matter at some particular point in an otherwise perfectly homogeneous early Universe. The pressure in the baryon–photon fluid associated with this overdensity drives a shock wave that expands at the sound speed c_s of the baryon–photon fluid (see figure 10 in Reference 24). Since the energy density at these early times is dominated by the photons, this sound speed c_s is just a bit smaller than $c/\sqrt{3}$, where c is the speed of light. When photons and baryons decouple, at a time $t_{\rm ls} \simeq 400{,}000$ years after the big bang (when the plasma temperature falls to $T \lesssim$ eV, allowing electrons to combine with nuclei), the shock-induced overdensity in the baryon–photon fluid has a radius on the order of $c_s t_{\rm ls}$.

The solution to the fluid equations with this Dirac delta function initial condition provides the Green function for the time evolution of primordial perturbations. When it is convolved with the primordial mass distribution, a realization of a random field, it provides the two-point correlation function at some later time. Thus, the two-point correlation function for the baryon density—and thus the total matter density, given that baryons constitute about one-fifth of the total matter density—has a bump at a comoving distance given by the sound horizon at matter–radiation equality. This bump shows up in the galaxy autocorrelation function at a distance of ∼150 Mpc. The relatively sharp feature in configuration space then gives rise to oscillatory structures in the Fourier domain. These are the celebrated baryon acoustic oscillations (BAOs) in the matter power spectrum.

3.1.2. H_0 from acoustic oscillations in the cosmic microwave background power spectrum. These oscillations also appear as the acoustic peaks in the angular power spectrum C_l of the CMB, since the photon density traces the baryon density at the time, ∼400,000 years after the big bang, at which the photons are released. In 1995, Reference 75 argued that measurement of these acoustic peaks could be used to determine the Hubble constant, along with the values of other cosmological parameters, by comparing theoretical calculations of C_l with measurements. The way that the Hubble constant comes out of this black box can be understood heuristically, however.

The multipole moment l_s of the first acoustic peak determines the angle subtended by the sound horizon at the surface of last scatter, given the correspondence $l_s \simeq 2/\theta_s$ between the angular variation θ of a spherical harmonic of multipole l. The angle subtended by the sound horizon is $\theta_s = r_s/D_A$, where D_A is the angular diameter distance to the CMB surface of last scatter, and $r_s \sim c_s t_{\rm dec}$ is the sound horizon. The parameter $\theta_s = (1.04109 \pm 0.00030) \times 10^{-2}$ is the most precisely determined parameter extracted from CMB measurements, determined to roughly one part in ten thousand.

More precisely, the sound horizon is obtained by integrating the sound speed $c_s(t)$ over time from the big bang to recombination. The comoving sound horizon can be represented by an integral,

$$r_s = \int_{z_{\rm ls}}^{\infty} \frac{c_s(z)\,dz}{H(z)} = \frac{c}{\sqrt{3}H_{\rm ls}} \int_{z_{\rm ls}}^{\infty} \frac{dz}{[\rho(z)/\rho(z_{\rm ls})]^{1/2}\,(1+R)^{1/2}}, \qquad 2.$$

over redshift z. Here, $z_{\rm ls} \simeq 1{,}080$ is the redshift at which CMB photons last scatter; $c_s(z) = c[3(1+R)]^{-1/2}$ is the sound speed of the baryon–photon fluid, with $R = (3/4)(\omega_b/\omega_\gamma)/(1+z)$; $\rho(z)$ is the total energy density at redshift z; and $\omega_b = \Omega_b h^2$ is the current physical baryon density (today), where $h \equiv H_0/(100\ {\rm km\ s^{-1}\ Mpc^{-1}})$ is a dimensionless Hubble constant. This ω_b is determined by the higher-peak structure in the CMB power spectrum far more precisely than Ω_b or H_0 separately. Planck's ΛCDM value is $\omega_b = 0.0224 \pm 0.0001$. At last scattering, $R \sim 0.5$, and it is smaller at higher redshifts. And $\omega_\gamma = 2.47 \times 10^{-5}$ is the physical photon energy density (76). The expansion rate at last scattering is

$$H_{\rm ls} = 100\,{\rm km\,s^{-1}\,Mpc^{-1}}\,\omega_r^{1/2}(1+z_{\rm ls})^2\sqrt{1+\frac{\omega_m}{\omega_r}\frac{1}{1+z_{\rm ls}}}, \qquad 3.$$

where $\omega_m = \Omega_m h^2$ is the physical nonrelativistic matter density today—this, again, is fixed fairly precisely by the higher-peak structure in the CMB; Planck's ΛCDM value is $\omega_m = 0.142 \pm 0.001$. In the standard cosmological model, the early-Universe energy density is $\rho(z) \propto \omega_m(1+z)^3 + \omega_r(1+z)^4$. The physical radiation density is

$$\omega_r = \left[1 + \frac{7}{8}N_{\rm eff}\left(\frac{4}{11}\right)^{4/3}\right]\omega_\gamma, \qquad 4.$$

where the second term accounts for additional nonrelativistic degrees of freedom. In the standard cosmological model, these include the three neutrino mass eigenstates, and $N_{\rm eff} = 3.06$ differs slightly from 3.00 because of the details of neutrino decoupling (77).

The (comoving) angular diameter distance to the surface of last scatter is then an integral,

$$D_A = \frac{c}{H_0}\int_0^{z_{\rm ls}} \frac{dz}{[\rho(z)/\rho_0]^{1/2}}, \qquad 5.$$

from recombination until the current time t_0, when the total energy density is ρ_0. The denominator here is $\rho(z)/\rho_0 = \Omega_m(1+z)^3 + (1-\Omega_m)(1+z)^{-3(1+w)}$ in the standard cosmological model with a dark energy equation-of-state parameter w. The cosmological constant corresponds to $w = -1$.

From $\theta_s = r_s/D_A$, we infer a Hubble constant,

$$H_0 = \sqrt{3}H_{\rm ls}\theta_s \frac{\int_0^{z_{\rm ls}} dz\ [\rho(z)/\rho_0]^{-1/2}}{\int_{z_{\rm ls}}^{\infty} dz\ [\rho(z)/\rho(z_{\rm ls})]^{-1/2}\,(1+R)^{-1/2}}, \qquad 6.$$

from the CMB. This is a function of ω_b through its appearance in R. There is a dependence on ω_m through its appearance in $\rho(z)/\rho(z_{\rm ls})$ at early times and in $H_{\rm ls}$. There is also a dependence on ω_m through the appearance of $\Omega_m = \omega_m/h^2$ in $\rho(z)$ at late times. Thus, strictly speaking, Equation 6 is an implicit equation for H_0, given that $h = H_0/(100\ {\rm km\ s^{-1}\ Mpc^{-1}})$ appears on the right-hand side. There is a dependence on ω_γ in the R and in the expression for ω_r, which also depends on $N_{\rm eff}$. The dependence on ω_r comes about in $H_{\rm ls}$ and in $\rho(z)$ at early times. The redshift $z_{\rm ls} \simeq 1{,}080$ of the last-scattering surface corresponds to the time when the rate for a photon to Thomson scatter from free electrons—which are becoming scarce as they become bound into hydrogen atoms—becomes smaller than the expansion rate. There is some dependence of $z_{\rm ls}$ on ω_b and ω_m that is taken into account in detailed analyses but that is too small to be relevant for the Hubble tension.

In practice, all of the unknown cosmological parameters are determined simultaneously by fitting precise numeric calculations of CMB power spectra to data. Still, ω_m and ω_b are determined primarily by characteristics in the CMB power spectrum, such as the Silk damping at higher l and the relative heights of the even- and odd-numbered peaks. The Hubble constant then follows from Equation 6. Through numeric differentiation of this expression, it can be found that the Hubble constant varies as $(\Delta H/H_0) \simeq 0.1\,(\Delta\omega_b/\omega_b)$ for small changes $\Delta\omega_b$ to the baryon density (holding all other parameters fixed) and with ω_m as $(\Delta H/H_0) \simeq -0.77\,(\Delta\omega_m/\omega_m)$ (keeping $\Omega_m = \omega_m/h^2$). This equation also illustrates how some simple modifications to the standard assumptions might affect the results. For example, if the number $N_{\rm eff}$ of relativistic degrees of freedom is increased, then the radiation density ω_r is accordingly increased, leading to a higher $H_{\rm ls}$ and thus a higher H_0. Alternatively, if we take $w < -1$, then the integral in the numerator of Equation 6 is increased, thus leading to a higher H_0.

3.1.3. Cosmic microwave background results. The first effort to determine H_0 from the CMB was in 2000 (78), but the results were not constraining because these initial measurements lacked enough information about the higher peaks in the CMB power spectrum to fix ω_m and ω_b. This was accomplished with NASA's Wilkinson Microwave Anisotropy Probe (WMAP), which arrived at $H_0 = 69.3 \pm 0.8$ km s^{-1} Mpc^{-1} (79) for their final mission value for the Hubble parameter [improving upon their first-year result, $H_0 = 73 \pm 5$ km s^{-1} Mpc^{-1} (80)].[1] Subsequently, the ESA's Planck satellite (4) provided power spectra to multipole moments $l \sim 2{,}500$, as opposed to $l \sim 800$ from WMAP, finding $H_0 = 67.4 \pm 0.5$ km s^{-1} Mpc^{-1}. These measurements were then complemented at even smaller angular scales by the Atacama Cosmology Telescope (ACT) and South Pole Telescope (SPT) Collaborations, which arrive at similar values of H_0 with errors below the scale of kilometers per second per megaparsec (81, 82).

3.1.4. Galaxy surveys and baryon acoustic oscillations. The sound horizon appears as a bump in the galaxy autocorrelation function at a distance scale ∼150 Mpc. In a galaxy-redshift survey, galaxy locations are parameterized by their position on the sky and by their redshift z, a proxy for the line-of-sight distance in the limit that peculiar velocities can be neglected. Two galaxies at similar redshift and some fixed angular separation have a physical separation proportional to the angular diameter distance $D_A(z)$, which is inversely proportional to H_0 and has a dependence on Ω_m (cf. Equation 1). A pair of galaxies along a given line of sight separated in redshift by Δz have a physical separation inversely proportional to the expansion rate $H(z) = H_0\sqrt{\Omega_m(1+z)^3+(1-\Omega)}$. To provide some indication of the state of the art, the transverse and radial BAO scales were measured in the Baryon Oscillation Spectroscopy Survey (BOSS) to ∼1.6% and ∼2.7% in redshift bins of width $\Delta z \sim 0.25$ (83). The degeneracy between H_0 and Ω_m in $H(z)$ or $D_A(z)$ is different at high and low redshifts and therefore can be broken by combining BAO measurements at different redshifts (e.g., figure 5 in Reference 5), and the BAO measurements now span the range $0.15 \lesssim z \lesssim 3$. Using the sound horizon inferred either from the CMB or from the value obtained by fixing the baryon density from BBN then allows a determination of the Hubble parameter with a similar error. In practice, galaxy survey analyses typically add to this pure-BAO measurement information from the correlation function shape and its time evolution and then combine with constraints to cosmological parameters from the CMB, weak gravitational lensing of galaxies or the CMB, or other measurements (for a comparison of the constraints derived under various assumptions, see, e.g., figure 20 in Reference 6). Currently, such BAO+ measurements provide

[1] Incidentally, WMAP's ∼1% measurement of H_0 improved upon the ∼10% forecast in Reference 75 because WMAP's capabilities turned out to be better than anticipated in that work, but also because the acoustic peak amplitudes turned out to be higher than expected with 1995 best-fit cosmological parameters.

(assuming a sound horizon determined from the CMB) H_0 values consistent with the CMB value and with errors below the scale of kilometers per second per megaparsec (5, 6).

3.2. Distance Scale of Matter–Radiation Equality

The Hubble parameter can also be constrained by the wavenumber k_{eq} of matter–radiation equality obtained from galaxy surveys. The primordial linear theory matter power spectrum $P(k)$ transitions from its large-wavelength ($k \to 0$) behavior $P(k) \propto k^{n_s}$ (with $n_s \simeq 0.96$ as the scalar spectral index) to $P(k) \propto k^{n_s-3}$ at $k \to \infty$ at a wavenumber k_{eq} corresponding to the mode that enters the horizon at matter–radiation equality. Given the rough coincidence between this distance scale and those corresponding to the sound horizon, the BAO wiggles in the power spectrum must be modeled out. Once they have been subtracted, though, the technique provides a sound-horizon-independent measurement of the Hubble parameter. This is the idea behind the ShapeFit algorithm (84), which in a preliminary application to BOSS data finds a low H_0. It is also the approach in Reference 85, which obtains a value of $H_0 = 64.8^{+2.2}_{-2.5}$ km s^{-1} Mpc^{-1}. However, this measurement assumes the standard ΛCDM power spectrum. If the early expansion history is changed in a manner suggested by EDE, then, as discussed below, the Hubble parameter inferred from this measurement is raised to a value consistent with the local SH0ES measurement (86).

4. THEORY AND MODELS

4.1. Early- Versus Late-Time Solutions

Barring a combination of systematics that address multiple types of observations, the Hubble tension implies some new physics beyond the ingredients (collisionless dark matter, a cosmological constant, and Standard Model interactions for baryons/photons) found in the standard cosmological model. Given that local measurements of the Hubble constant are fairly straightforward, the aim of most solutions to the Hubble tension is to introduce new physics that increases the value of H_0 inferred from the CMB.

These solutions are typically categorized as late-time or early-time—a classification scheme that can be understood from Equation 5. Late-time solutions postulate that the energy density in the post-recombination Universe is smaller than in the Standard Model, holding the current density fixed: that is, $\rho(z)/\rho_0(z) \leq [\rho(z)/\rho_0(z)]_{\text{standard}}$ (cf. Equation 6). This increases the comoving distance to the surface of last scatter and thus leads to a larger H_0. Early-time solutions postulate that the energy density is somehow increased before recombination so that the sound horizon at recombination is decreased. We will also discuss models that decrease the sound horizon by changing the physics of the baryon–photon fluid.

Given the plethora of models and the continued inventiveness of theorists, care should be taken in making blanket statements. Still, there are theoretical reasons that make late-time solutions unpalatable and empirical constraints that make them elusive. With a late-time solution, the energy density at times between decoupling and now must be kept smaller than that in the Standard Model, but the energy density today must be kept fixed (87). Given that the scaling of the radiation and matter densities with redshift is known, this requires some exotic matter whose energy density increases with time. This is most easily accomplished by postulating that the cosmological constant is a phantom field (88), a fluid with an equation-of-state parameter $w = p/\rho < -1$, where p and ρ are the dark energy pressure and energy density. This, however, implies a fluid that violates the strong energy condition; that is, it effectively creates energy out of nowhere. This seems strange, but is this what the Hubble tension is telling us? Even if we are willing to accept a violation of the strong energy condition, such models are difficult to reconcile with the sound horizon seen

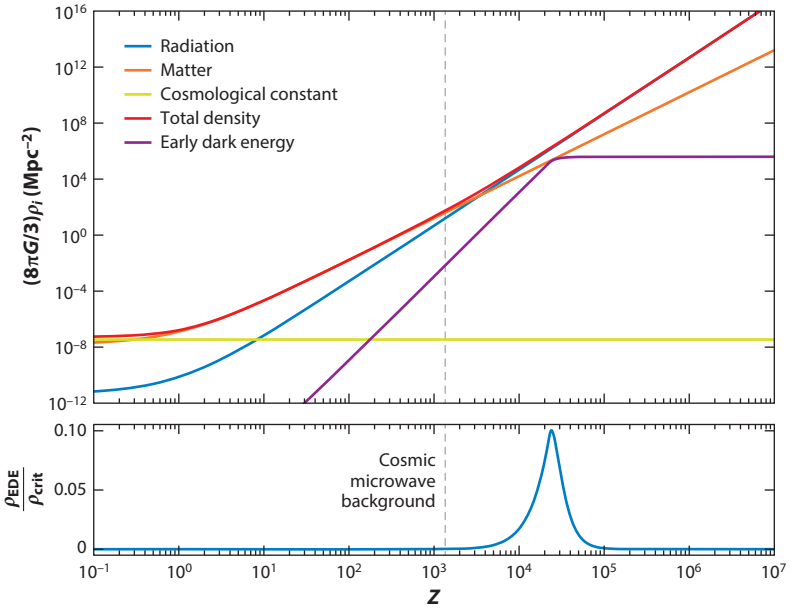

Figure 6

The evolution of the energy densities of radiation, nonrelativistic matter (baryons and cold dark matter), and the cosmological constant as a function of redshift (so time increases to the left, with the big bang far off to the right and today off to the left). Also shown is the energy density postulated for early dark energy (EDE). The bottom panel shows the fractional contribution of EDE to the total energy density. The EDE curves are schematic—the key point is that it contributes ∼10% a bit before recombination but is otherwise dynamically unimportant. Figure courtesy of T. Karwal.

in the galaxy correlation function (89, 90). They are also difficult to reconcile with constraints to the equation-of-state parameter w inferred recently from SNe Ia at high redshifts (25).

4.2. Early Dark Energy

The basic idea behind EDE is to postulate some exotic fluid that contributes ∼10% of the total energy density of the Universe briefly before recombination and then has an energy density that decays faster than radiation at late time, so that it leaves the late evolution of the Universe unchanged, as illustrated in **Figure 6**. This increases $\rho(z)/\rho(z_{ls})$ in the denominator of Equation 6, thus leading to a higher H_0. Although the basic idea is simple, specific models are highly constrained by the very well-measured structure of the high-l peaks in the CMB power spectra. Fourier modes of the density field that correspond to the highest multipole moments ($l \sim 3{,}000$) probed by current measurements entered the cosmological horizon and became dynamical at a redshift $z \sim 10^6$, when the Universe was only about a year old. The measured CMB power spectrum thus constrains the expansion history to far earlier times than the time of last scattering. Moreover, a fluid with a density that evolves with time implies, for a relativistically invariant theory, the possibility of spatial fluctuations in the EDE density. This, along with the already complicated interplay between baryon–photon acoustic waves, dark matter, neutrinos, and the gravitational field, implies that any physical model for EDE will be highly constrained.

Even so, it was found in Reference 15 that physical models of EDE could resolve the Hubble tension. **Figure 7** shows the results reported there for EDE models in which the EDE density

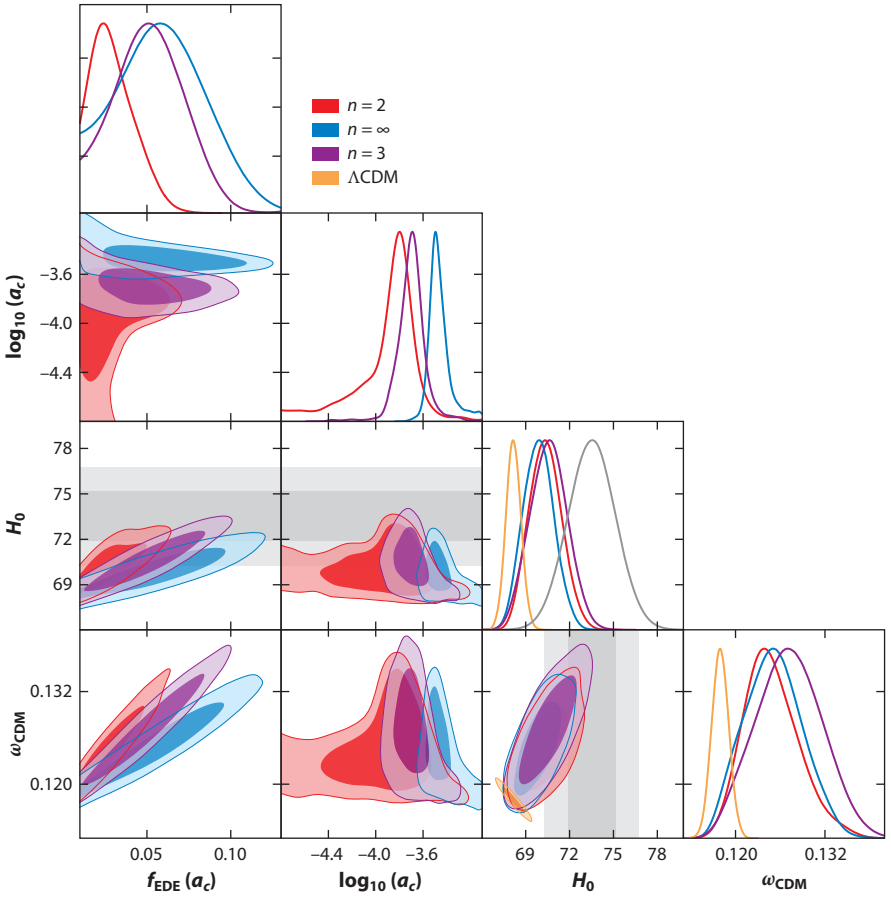

Figure 7

Likelihood contours from Reference 143 for ΛCDM and EDE in a subset of the nine-dimensional parameter space. These are likelihoods for the model given data from CMB and LSS measurements as of late 2018. The nine parameters include the six ΛCDM parameters (Ω_m, h, A_s, Ω_b, n_s, τ) along with three EDE parameters: the fractional contribution $f_{\rm EDE}(a_c)$ to the total cosmic density at the scale factor a_c (normalized to unity today) at which this fractional density peaks, and a third parameter that quantifies the sharpness of the transition of EDE from its early-time constant-density behavior to its later decay. Each panel shows the likelihood contours in a given two-dimensional slice of the full parameter space after marginalizing over the other seven parameters. At the top of each column is the likelihood for the given parameter after marginalizing over all other parameters. The gray bands and curves indicate the likelihoods for the Hubble constant H_0 from local measurements. The orange contours show the standard ΛCDM results and indicate the preference of CMB/LSS data for a low Hubble parameter. The other three sets of contours describe EDE models in which the EDE decays with scale factor a at late times as $a^{-6n/(n+1)}$. It is seen that EDE expands the allowed parameter space to regions that overlap the local values of H_0. Although it cannot be inferred from the figure, it can be checked that the regions of the EDE parameter space that accommodate a larger H_0 do so with a reduced χ^2 similar to that for the best-fit ΛCDM model. Abbreviations: CDM, cold dark matter; EDE, early dark energy; CMB, cosmic microwave background; LSS, Large Scale Structure. The dark- and light-shaded colors correspond, respectively, to 2σ and 3σ regions of the parameter space. Figure adapted from Reference 143.

decays with scale factor a at late times as $a^{-6n/(n+1)}$. As can be seen from the H_0 likelihood distribution, the addition of EDE allowed (as of late 2018) for larger values of H_0, which overlap the range of values allowed by local measurements, to be inferred from CMB/Large Scale Structure (LSS) data. Moreover, the best-fit EDE model had a similar reduced χ^2 as the best-fit ΛCDM model. The results shown here are for oscillating-field and slow-roll models for EDE, both of which can be described within the required precisions with the generalized dark matter (GDM) formalism.

4.2.1. Oscillating-field models. Oscillating scalar fields underlie many of the EDE models that have been explored. Here, a scalar field ϕ is postulated with a confining potential (91),

$$V(\phi) = \Lambda_{\rm EDE}^4 \left[1 - \cos(\phi/f_{\rm EDE})\right]^n, \qquad 7.$$

with an energy scale $\Lambda_{\rm EDE} \sim$ eV so that the energy density is in the ballpark of that of the Universe before recombination. Although this potential was postulated (91) in an ad hoc fashion, Reference 92 argues that it may arise in string theory. If the initial field value is $\phi/f \sim \pi$, then the field is initially frozen and behaves gravitationally like a cosmological constant. Later, though, the field begins to oscillate about its minimum with an equation-of-state parameter $w_{\rm EDE} = (n-1)/(n+1)$ and an energy density that decays with scale factor a as $\rho_{\rm EDE} \propto a^{-6n/(n+1)}$ (93, 94). Thus, for $n > 1$, the EDE density decays faster than that of radiation, as needed. Another similar possibility is to simply take the potential to be $V(\phi) \propto \phi^{2n}$ (95). Oscillating-field models are parameterized (for fixed n) by the energy density $\Lambda_{\rm EDE}$, the decay constant $f_{\rm EDE}$, and the initial field value ϕ_i. The power law index n can be considered as a fourth parameter.

4.2.2. Slow-roll models. Another possibility (15, 96) is a scalar field with a smooth slow-roll potential like those considered for inflation or quintessence. For example, a potential that asymptotes to a power law ϕ^n for large positive ϕ but then asymptotes to zero for large negative ϕ will have an energy density that is constant at early times and then scales as $\rho \propto a^{-6}$ at late times. Reference 96 discusses characteristics of EDE potentials and also generalizes to models with nontrivial kinetic terms.

4.2.3. Generalized early dark energy. EDE models can also be approached in a slightly more model-independent way using the GDM approach (97). Here, it is noted that communication between the dark sector (dark matter, dark energy, EDE) and the gravitational fields occurs in the Einstein equations only through the stress tensor that can be parameterized in terms of a fluid density, pressure, sound speed, and viscosity parameter. With this approach, the EDE can be described as a fluid with these parameters. The approach can be beneficial since codes that modify the standard cosmological Boltzmann codes (98–101) to include rapidly oscillating fields are numerically challenging given the wide separation between the oscillation and expansion time scales (102). Reference 15 shows how the parameters of the oscillating-field model can be mapped to GDM parameters, and Reference 103 then maps EDE-like physics in terms of a GDM-like parameterization.

4.2.4. Specific implementations. One of the curious aspects of EDE models is the coincidence between the time at which EDE becomes dynamical and the epoch of matter–radiation equality. It may be possible to connect these in chameleon models (104) and possibly in some of the alternative gravity models reviewed below. This epoch also coincides with the time at which the heavier neutrino mass eigenstate(s) becomes nonrelativistic, a realization capitalized upon in Reference 105.

References 106 and 107 show that the friction required for slow-roll models may be induced by coupling an axion field to a thermal bath in non-Abelian theories. The idea of interacting thermal baths also plays a role in the scenario of Reference 108. Here, interactions of strongly

coupled radiation are mediated by a force carrier that becomes nonrelativistic at a temperature $T \sim$ eV. The mediator then deposits its entropy into the lighter species, thus providing a step in the effective number $N_{\rm eff}$ of relativistic degrees of freedom. This provides a higher energy density just before recombination while avoiding the problems at high l in the CMB power spectrum associated with an increased $N_{\rm eff}$.

4.3. Other Early Dark Energy Observables

If the Hubble tension is solved by EDE, it is natural to inquire whether the new physics associated with EDE has any other observable consequences beyond the impact on the expansion history. Given the disparity in models, there is no general consequence, but several possibilities have been discussed.

4.3.1. Cosmic birefringence. If a scalar field $\phi(x)$ is coupled to the electromagnetic field-strength tensor $F_{\mu\nu}(x)$ through a term $[\phi(x)/m_{\rm Pl}]\epsilon^{\mu\nu\rho\sigma}F_{\mu\nu}F_{\rho\sigma}$ in the Lagrangian, then time evolution of the scalar field yields a difference in the propagation speeds for right- and left-circularly polarized electromagnetic waves and, thus, a frequency-independent rotation of the linear polarization of an electromagnetic wave (109–111). One possibility for such a time-evolving scalar field is quintessence, a candidate for dark energy (13, 111). Another is a slowly rolling scalar field associated with EDE (112, 113). In either case, the rotation angle is $\Delta\phi/m_{\rm Pl}$, where $\Delta\phi$ is the change in ϕ between the emission and observation of the electromagnetic wave [although, strictly speaking, this result is altered if some of the rotation occurs before recombination (113)]. This cosmic birefringence (CB) leads to parity-breaking EB and TB [where T, E, and B refer to the temperature and parity-even and parity-odd polarization modes (114, 115)] correlations in the CMB power spectra (116, 117). The association of CB with EDE can be distinguished from late-Universe CB-inducing physics by the absence of CB observed in late-Universe probes like those that seek CB in the CMB reionization bump (118) or in kinetic Sunyaev–Zeldovich tomography (119, 120).

4.3.2. Nonlinear evolution of oscillating early dark energy field. If EDE is due to an oscillating field, nonlinear evolution of the scalar-field perturbations may lead to strong instabilities that subsequently generate nonlinear spatially inhomogeneous dynamics or soliton-like structures, which then evolve as a subdominant dark matter component (95, 121). There is also a possibility that fluctuations in the initial field value may give rise to isocurvature perturbations (121).

4.3.3. The light horizon. Changes to the early expansion history will affect the light horizon at decoupling probed by the acoustic peaks in the CMB B-mode power spectrum (122). These B modes are induced by inflationary GWs, but their amplitude depends on the energy scale of inflation, which is still undetermined. Observation of these peaks is conceivable with a ground-based Stage IV CMB experiment if the B-mode amplitude is near the current upper limit. However, a space-based experiment, like PICO (123), may be required if the B-mode amplitude is smaller by an order of magnitude, and the measurement cannot be done if the GW amplitude is any smaller.

4.3.4. Recurrent cosmological-constant-like behavior? If the Hubble tension is due to EDE, it also suggests—in combination with evidence for accelerated expansion today (11, 12) and for inflation in the early Universe—the possibility of recurrent periods of cosmological-constant-like behavior throughout the history of the Universe. This possibility was anticipated in work on tracking-field models (124, 125): quintessence models in which the potential is such that the energy density is always a (roughly) fixed fraction of the energy density of the dominant matter

component (radiation or matter). If, however, small wiggles are added to this potential, then the energy density in the quintessence field can occasionally jump and behave briefly like a cosmological constant before decaying away. The possibility was also anticipated in a string axiverse scenario (91). Here, in each logarithmic time interval in the Universe's history, there is an axion-like field, with potential as in Equation 7, that becomes dynamical. The initial field value is chosen from random, and if it is sufficiently displaced from the minimum, it can briefly behave dynamically like a cosmological constant. This scenario also resembles assisted quintessence, which is explored in connection with EDE in Reference 126. The idea of recurring cosmological constants motivates the search for other times in cosmic history at which the expansion rate can be probed. BBN constrains the expansion rate a few minutes after the big bang. Reference 127 discusses the possibility of probing the expansion history at redshifts $z \sim 17$ with the global 21-cm intensity as measured, for example, by EDGES (128). Velocity acoustic oscillations—oscillations in the 21-cm angular power spectrum induced by spatial modulation of star formation induced by baryon–dark matter relative velocities—may also probe the expansion history at similar redshifts (129–131). However, more can probably be done along these lines.

4.4. Other Early-Universe Solutions

4.4.1. Modified gravity. Modifications to gravity are notoriously difficult: Since modifications to the Einstein–Hilbert action generically make the scalar degree of freedom (at least, and sometimes also the vector degrees of freedom) in the metric dynamical, there is no obvious way to perturb away from general relativity. Nevertheless, the accelerated cosmic expansion, the persistent mystery of dark matter, and now GW measurements that probe previously inaccessible regions of strong-field gravity have yielded an active marketplace of alternative gravity theories that can be explored in connection with the Hubble tension (132–139).

For example, Reference 132 takes a phenomenological approach to modified gravity in which the evolution of cosmological perturbations takes on a parameterized departure from those in general relativity. In relativistic cosmological perturbation theory, there are two scalar potentials, Φ and Ψ (in conformal Newtonian gauge), that generalize the gravitational potential in Newtonian gravity. The equations that relate these to the energy-density perturbation, pressure, and anisotropic stress are modified in two ways. First, Newton's constant G in the Fourier space equations is multiplied by a function $\mu(a, k)$ of the scale factor a and wavenumber k. And second, the cosmic slip $\Phi - \Psi$ (sourced by the anisotropic stress) is replaced by $\Phi - \gamma(a, k)\Psi$. GR is recovered in the limits $\gamma \to 1$ and $\mu \to 1$. A departure of μ from unity at early times affects the evolution of the gravitational fields so that the phase of the acoustic oscillations is shifted in a way that mimics a shift in the sound horizon.

In conformally coupled gravity, the Ricci scalar R in the Einstein–Hilbert action is multiplied by a function $(1 + \xi\phi^2/m_{\rm Pl}^2)$ of a scalar field ϕ with $\xi = -1/6$, so that the scalar is conformally coupled. The equation of motion for the scalar field is $\ddot{\phi} + 3H\dot{\phi} - \xi R\phi = 0$. At early times, during radiation domination, $H^2 \gg R$, and the scalar field is frozen at its initial value. Near the transition to matter domination, when R approaches H^2, the field starts to roll to its minimum (leaving gravity as it is today) and then has an energy density that decays away as $\rho_\phi \propto a^{-9/2}$ in the matter-dominated era (138).

4.4.2. Changing $N_{\rm eff}$. The idea to reduce the sound horizon by increasing the early-Universe expansion rate preceded EDE models; it was noted that an increase in the number $N_{\rm eff}$ of relativistic degrees of freedom would allow for a larger Hubble constant (8), but this solution did not provide a good fit to CMB data given that an increased $N_{\rm eff}$ affects the higher-l modes in the CMB that probe redshifts up to $z \sim 10^6$. A fractional increase in $N_{\rm eff}$ in the range of 0.2 to 0.4 is still

allowed and could alleviate the Hubble tension. Detection of an additional, sterile neutrino would reopen this solution space.

4.4.3. Changing physics of the baryon–photon fluid. Models with interacting neutrinos have also been explored (140). However, they modify the sound horizon through dynamics of the perturbations rather than by increasing the expansion rate, and thus they probably should not be classified as EDE models. They also run up against laboratory constraints to neutrino properties (141). Primordial magnetic fields have also been suggested as a solution to the Hubble tension (142), but the viability of the idea awaits a more detailed calculation of the evolution of perturbations.

4.5. Recent Results from Cosmic Microwave Background/Large Scale Structure Data

There is now a large literature devoted to testing various EDE models with the ever-increasing products of ongoing galaxy surveys and CMB experiments. The results of Reference 143 shown in **Figure 7** have been reproduced, updated, and expanded upon with different data sets. We do not review this work in detail here, as the literature is large and the situation rapidly evolving with new data sets.

Since the level at which EDE models differ from ΛCDM is at the $\sim 3\sigma$ level, small changes in analyses or model assumptions that one might guess were below the radar can actually affect the conclusions. For example, the galaxy-clustering constraint to H_0 changes by about 0.7 km s^{-1} Mpc^{-1} if the dark energy is assumed to be a cosmological constant or described by a more general equation-of-state parameter (6). Similar shifts arise from different assumptions about still-undetermined neutrino masses. Although these shifts are small, at the 1σ level, they can change a result from the $>3\sigma$ threshold to a $<3\sigma$ result. At this level, conclusions can also depend on the interpretation of the statistics. For example, References 144–146 argue that current data favor ΛCDM over EDE at the $\gtrsim 3\sigma$ level, while others (147, 148) warn that the conclusions may reflect the choice of priors.

Perhaps the most intriguing results at the time of writing are those reported in References 149 and 150. They indicate that new measurements of small-scale polarization from ACT Data Release 4 (81) favor EDE over ΛCDM at the $\gtrsim 3\sigma$ level. The results should be considered as provisional given some possible inconsistencies between Planck and ACT measurements. Still, the results, based on a fraction of current polarization data, suggest that forthcoming experiments, like the Simons Observatory and CMB-S4 (if not ACT/SPT data obtained even sooner), should distinguish EDE from ΛCDM with high statistical significance.

Perhaps the most important takeaway is that 4 years later, with several new data sets [especially for small-scale CMB fluctuations, which were anticipated (143) to provide the most stringent tests of EDE], EDE remains consistent and even possibly favored over ΛCDM. We refer readers interested in a more detailed discussion of the statistical techniques, tests, and data sets to Reference 22 and to Reference 19 for a comprehensive tour of EDE models.

5. CONCLUSIONS

The discrepancy between local determinations of the cosmic expansion rate based on distance and redshift measurements and the expansion rate inferred from CMB data and galaxy clustering has over time become statistically more significant with new data and simultaneously has survived careful scrutiny of the relevant measurements and analyses. This Hubble tension is not solved by any quick fix to the standard cosmological model. If it were the other way (a lower local H_0), it could

be accommodated with the types of models for (late-time) dark energy that have been considered for 20 years. Analogous cosmological tensions in the past have yielded to new insights into stellar populations (to explain Hubble's anomalously large initial expansion rate) and fundamental physics (the 1990s discrepancy between the Hubble constant and age of the Universe, which was explained ultimately by the discovery of the cosmological constant). Although it remains to be seen how the current Hubble tension will be resolved, it is likely to provide profound new insights into astrophysics or physics.

The most promising new-physics explanation for the Hubble tension is some new early-Universe physics that decreases the sound horizon. The most popular playground for such ideas has been EDE, which reduces the sound horizon by increasing the expansion rate, but there are other models that involve, for example, modified gravity or changes to the primordial plasma physics. Any such model, though, is highly constrained by the data—the model must preserve the excellent agreement between disparate and precise data sets and the canonical ΛCDM model. Still, there are models that work and, moreover, remain viable even after comparison with several precise new data sets. Unlike the last (1990s) Hubble tension, which was resolved ultimately by one number—the cosmological constant—the specification of EDE models is more complicated and thus not as easily digested by theorists. Still, it is up to data rather than our prejudices to decide.

Fortunately, the next steps in exploring the Hubble tension are clear. Moreover, the required observational infrastructure is already in place, as it coincides largely with that assembled to study (late-Universe) dark energy and inflation. Ultimately, we must continue to explore astrophysical and measurement uncertainties. As we have learned over and over in cosmology, there is no single bullet: Robust conclusions are reached only with multiple observational avenues and a tightly knit web of calibrations, cross-calibrations, and consistency checks.

SUMMARY POINTS

1. The values of the Hubble constant inferred from cosmic microwave background (CMB) measurements and galaxy surveys disagree at the $\gtrsim 5\sigma$ level with those obtained from measurements of distances and redshifts in the local Universe.
2. The discrepancy has not yielded to any simple explanations in terms of systematic effects despite considerable scrutiny of the CMB and local measurements.
3. Of the many models with new physics explored to explain this Hubble tension, those that involve modifications to early-Universe dynamics seem best able to satisfy the panoply of cosmological constraints.
4. Although there have been some hints of early dark energy (EDE) in recent analyses, current CMB data are not yet precise and robust enough to distinguish EDE models from the standard Lambda cold dark matter (ΛCDM) model.

FUTURE ISSUES

1. Improved local measurements are needed to refine the Hubble constant while maintaining control of systematic errors with ∼1% as a target goal and independent tests at ∼3% precision providing valuable cross-checks. Greater specificity is needed to describe any systematic errors that would evade present detection and affect multiple, independent measures.

2. Forthcoming experiments that more precisely map the CMB polarization on smaller angular scales will be required to test EDE and other new-physics models for the Hubble tension.
3. If future measurements favor EDE models over the standard ΛCDM model, it will be important to understand more deeply the nature of the new physics that provides EDE-like dynamics in the early Universe and to explore other times when dark energy may have affected dynamics of the Universe.
4. It will also be important to think about laboratory, or other noncosmological, tests of any such new physics.

DISCLOSURE STATEMENT

The authors are not aware of any affiliations, memberships, funding, or financial holdings that might be perceived as affecting the objectivity of this review.

ACKNOWLEDGMENTS

We thank Licia Verde for comments on an earlier draft. M.K. was supported by the National Science Foundation (grant 2112699) and the Simons Foundation.

LITERATURE CITED

1. Asimov I. *Asimov's Chronology of Science & Discovery: Updated and Illustrated*. New York: Harper-Collins (1994)
2. Freedman WL, et al. *Astrophys. J.* 553:47 (2001)
3. Freedman WL, et al. *Astrophys. J. Lett.* 758:24 (2012)
4. Aghanim N, et al. *Astron. Astrophys.* 641:A6 (2020). Erratum. *Astron. Astrophys.* 652:C4 (2021)
5. Alam S, et al. *Phys. Rev. D* 103:083533 (2021)
6. Abbott TMC, et al. *Phys. Rev. D* 105:023520 (2022)
7. Riess AG, et al. *Astrophys. J.* 730:119 (2011). Erratum. *Astrophys. J.* 732:129 (2011)
8. Riess AG, et al. *Astrophys. J.* 826:56 (2016)
9. Riess AG, et al. *Astrophys. J. Lett.* 934:L7 (2022)
10. Abdalla E, et al. *J. High Energy Astrophys.* 34:49 (2022)
11. Perlmutter S, et al. *Astrophys. J.* 517:565 (1999)
12. Riess AG, et al. *Astron. J.* 116:1009 (1998)
13. Caldwell RR, Kamionkowski M. *Annu. Rev. Nucl. Part. Sci.* 59:397 (2009)
14. Karwal T, Kamionkowski M. *Phys. Rev. D* 94:103523 (2016)
15. Poulin V, et al. *Phys. Rev. D* 98:083525 (2018)
16. Bernal JL, Verde L, Riess AG. *J. Cosmol. Astropart. Phys.* 1610:019 (2016)
17. Verde L, Treu T, Riess AG. *Nat. Astron.* 3:891 (2019)
18. Knox L, Millea M. *Phys. Rev. D* 101:043533 (2020)
19. Di Valentino E, et al. *Class. Quant. Grav.* 38:153001 (2021)
20. Shah P, Lemos P, Lahav O. *Astron. Astrophys. Rev.* 29:9 (2021)
21. Efstathiou G. *Mon. Not. R. Astron. Soc.* 505:3866 (2021)
22. Schöneberg N, et al. *Phys. Rep.* 984:1 (2022)
23. Frieman J, Turner M, Huterer D. *Annu. Rev. Astron. Astrophys.* 46:385 (2008)
24. Weinberg DH, et al. *Phys. Rep.* 530:87 (2013)
25. Brout D, et al. *Astrophys. J.* 938:110 (2022)
26. Riess AG, et al. *Astrophys. J.* 876:85 (2019)

27. Leavitt HS, Pickering EC. *Harv. Coll. Obs. Circ.* 173:1 (1912)
28. Eddington AS. *The Observatory* 40:290 (1917)
29. Christy RF. *Annu. Rev. Astron. Astrophys.* 4:353 (1966)
30. Pesce DW, et al. *Astrophys. J. Lett.* 891:L1 (2020)
31. Riess AG, et al. *Astrophys. J.* 861:126 (2018)
32. Riess AG, et al. *Astrophys. J. Lett.* 908:L6 (2021)
33. Yuan W, Riess AG, Casertano S, Macri LM. *Astrophys. J. Lett.* 940:L17 (2022)
34. Scolnic DM, et al. *Astrophys. J.* 859:101 (2018)
35. Burns CR, et al. *Astrophys. J.* 869:56 (2018)
36. Feeney SM, Mortlock DJ, Dalmasso N. *Mon. Not. R. Astron. Soc.* 476:3861 (2018)
37. Javanmardi B, et al. *Astrophys. J.* 911:12 (2021)
38. Breuval L, et al. *Astrophys. J.* 939:89 (2022)
39. Riess AG, et al. *Astrophys. J.* 938:36 (2022)
40. Hoyt TJ, et al. *Astrophys. J.* 915:34 (2021)
41. Freedman WL, et al. *Astrophys. J.* 882:34 (2019)
42. Anand GS, et al. *Astron. J.* 162:80 (2021)
43. Blakeslee JP, et al. *Astrophys. J.* 911:65 (2021)
44. Li S, Casertano S, Riess AG. *Astrophys. J.* 939:96 (2022)
45. Soltis J, Casertano S, Riess AG. *Astrophys. J. Lett.* 908:L5 (2021)
46. Peterson ER, et al. *Astrophys. J.* 938:112 (2022)
47. Brownsberger S, et al. arXiv:2110.03486 [astro-ph.CO] (2021)
48. Schutz BF. *Nature* 323:310 (1986)
49. Abbott BP, et al. *Phys. Rev. Lett.* 119:161101 (2017)
50. Abbott BP, et al. *Astrophys. J. Lett.* 848:L12 (2017)
51. Abbott BP, et al. *Astrophys. J. Lett.* 848:L13 (2017)
52. Abbott BP, et al. *Nature* 551:85 (2017)
53. Chen HY, Fishbach M, Holz DE. *Nature* 562:545 (2018)
54. Soares-Santos M, et al. *Astrophys. J. Lett.* 876:L7 (2019)
55. Huang CD, et al. *Astrophys. J.* 889:5 (2020)
56. Tonry J, Schneider DP. *Astron. J.* 96:807 (1988)
57. Garnavich P, et al. arXiv:2204.12060 [astro-ph.CO] (2022)
58. Refsdal S. *Mon. Not. R. Astron. Soc.* 128:307 (1964)
59. Vanderriest C, et al. *Astron. Astrophys.* 215:1 (1989)
60. Keeton CR, Kochanek CS. *Astrophys. J.* 487:42 (1997)
61. Schechter PL, et al. *Astrophys. J. Lett.* 475:L85 (1997)
62. Koopmans LVE, et al. *Astrophys. J.* 599:70 (2003)
63. Wong KC, et al. *Mon. Not. R. Astron. Soc.* 498:1420 (2020)
64. Falco EE, Gorenstein MV, Shapiro II. *Astrophys. J. Lett.* 289:L1 (1985)
65. Birrer S, et al. *Astron. Astrophys.* 643:A165 (2020)
66. Millon M, et al. *Astron. Astrophys.* 639:A101 (2020)
67. Jimenez R, Loeb A. *Astrophys. J.* 573:37 (2002)
68. Stern D, et al. *J. Cosmol. Astropart. Phys.* 1002:008 (2010)
69. Moresco M, et al. *J. Cosmol. Astropart. Phys.* 1208:006 (2012)
70. Moresco M, et al. *Astrophys. J.* 898:82 (2020)
71. Borghi N, et al. *Astrophys. J.* 927:164 (2022)
72. O'Malley EM, Gilligan C, Chaboyer B. *Astrophys. J.* 838:162 (2017)
73. Jimenez R, et al. *J. Cosmol. Astropart. Phys.* 1903:043 (2019)
74. Bernal JL, et al. *Phys. Rev. D* 103:103533 (2021)
75. Jungman G, Kamionkowski M, Kosowsky A, Spergel DN. *Phys. Rev. D* 54:1332 (1996)
76. Fixsen DJ, et al. *Astrophys. J.* 473:576 (1996)
77. Dodelson S, Turner MS. *Phys. Rev. D* 46:3372 (1992)
78. Jaffe AH, et al. *Phys. Rev. Lett.* 86:3475 (2001)

79. Bennett CL, et al. *Astrophys. J. Suppl.* 208:20 (2013)
80. Spergel DN, et al. *Astrophys. J. Suppl.* 148:175 (2003)
81. Aiola S, et al. *J. Cosmol. Astropart. Phys.* 2012:047 (2020)
82. Dutcher D, et al. *Phys. Rev. D* 104:022003 (2021)
83. Ross AJ, et al. *Mon. Not. R. Astron. Soc.* 464:1168 (2017)
84. Brieden S, Gil-Marín H, Verde L. *Phys. Rev. D* 104:L121301 (2021)
85. Philcox OHE, et al. *Phys. Rev. D* 106:063530 (2022)
86. Smith TL, Poulin V, Simon T. arXiv:2208.12992 [astro-ph.CO] (2022)
87. Poulin V, Boddy KK, Bird S, Kamionkowski M. *Phys. Rev. D* 97:123504 (2018)
88. Caldwell RR. *Phys. Lett. B* 545:23 (2002)
89. Efstathiou G. *Mon. Not. R. Astron. Soc.* 505:3866 (2021)
90. Keeley RE, Shafieloo A. arXiv:2206.08440 [astro-ph.CO] (2022)
91. Kamionkowski M, Pradler J, Walker DGE. *Phys. Rev. Lett.* 113:251302 (2014)
92. McDonough E, Scalisi M. arXiv:2209.00011 [hep-th] (2022)
93. Turner MS. *Phys. Rev. D* 28:1243 (1983)
94. Johnson MC, Kamionkowski M. *Phys. Rev. D* 78:063010 (2008)
95. Agrawal P, Cyr-Racine FY, Pinner D, Randall L. arXiv:1904.01016 [astro-ph.CO] (2019)
96. Lin MX, Benevento G, Hu W, Raveri M. *Phys. Rev. D* 100:063542 (2019)
97. Hu W. *Astrophys. J.* 506:485 (1998)
98. Bertschinger E. arXiv:astro-ph/9506070 (1995)
99. Seljak U, Zaldarriaga M. *Astrophys. J.* 469:437 (1996)
100. Lewis A, Challinor A, Lasenby A. *Astrophys. J.* 538:473 (2000)
101. Lesgourgues J. Report CERN-PH-TH/2011-081, CERN, Geneva (2011)
102. Hlozek R, Marsh DJE, Grin D. *Mon. Not. R. Astron. Soc.* 476:3063 (2018)
103. Sabla VI, Caldwell RR. *Phys. Rev. D* 106:063526 (2022)
104. Karwal T, et al. *Phys. Rev. D* 105:063535 (2022)
105. Sakstein J, Trodden M. *Phys. Rev. Lett.* 124:161301 (2020)
106. Berghaus KV, Karwal T. *Phys. Rev. D* 101:083537 (2020)
107. Berghaus KV, Karwal T. arXiv:2204.09133 [astro-ph.CO] (2022)
108. Aloni D, et al. *Phys. Rev. D* 105:123516 (2022)
109. Harari D, Sikivie P. *Phys. Lett. B* 289:67 (1992)
110. Carroll SM, Field GB, Jackiw R. *Phys. Rev. D* 41:1231 (1990)
111. Carroll SM. *Phys. Rev. Lett.* 81:3067 (1998)
112. Capparelli LM, Caldwell RR, Melchiorri A. *Phys. Rev. D* 101:123529 (2020)
113. Murai K, Naokawa F, Namikawa T, Komatsu E. arXiv:2209.07804 [astro-ph.CO] (2022)
114. Kamionkowski M, Kosowsky A, Stebbins A. *Phys. Rev. D* 55:7368 (1997)
115. Zaldarriaga M, Seljak U. *Phys. Rev. D* 55:1830 (1997)
116. Lue A, Wang LM, Kamionkowski M. *Phys. Rev. Lett.* 83:1506 (1999)
117. Lepora NF. arXiv:gr-qc/9812077 (1998)
118. Liu GC, Lee S, Ng KW. *Phys. Rev. Lett.* 97:161303 (2006)
119. Hotinli SC, Holder GP, Johnson MC, Kamionkowski M. *J. Cosmol. Astropart. Phys.* 2210:026 (2022)
120. Lee N, Hotinli SC, Kamionkowski M. *Phys. Rev. D* 106:083518 (2022)
121. Smith TL, Poulin V, Amin MA. *Phys. Rev. D* 101:063523 (2020)
122. Jeong D, Kamionkowski M. *Phys. Rev. Lett.* 124:041301 (2020)
123. Hanany S, et al. arXiv:1902.10541 [astro-ph.IM] (2019)
124. Griest K. *Phys. Rev. D* 66:123501 (2002)
125. Dodelson S, Kaplinghat M, Stewart E. *Phys. Rev. Lett.* 85:5276 (2000)
126. Sabla VI, Caldwell RR. *Phys. Rev. D* 103:103506 (2021)
127. Hill JC, Baxter EJ. *J. Cosmol. Astropart. Phys.* 1808:037 (2018)
128. Bowman JD, et al. *Nature* 555:67 (2018)
129. Muñoz JB. *Phys. Rev. Lett.* 123:131301 (2019)
130. Muñoz JB. *Phys. Rev. D* 100:063538 (2019)

131. Sarkar D, Kovetz ED. *Phys. Rev. D* 107:023524 (2023)
132. Lin MX, Raveri M, Hu W. *Phys. Rev. D* 99:043514 (2019)
133. Braglia M, Ballardini M, Finelli F, Koyama K. *Phys. Rev. D* 103:043528 (2021)
134. Braglia M, et al. *Phys. Rev. D* 102:023529 (2020)
135. Ballesteros G, Notari A, Rompineve F. *J. Cosmol. Astropart. Phys.* 2011:024 (2020)
136. Ballardini M, et al. *J. Cosmol. Astropart. Phys.* 2010:044 (2020)
137. Zumalacarregui M. *Phys. Rev. D* 102:023523 (2020)
138. Abadi T, Kovetz ED. *Phys. Rev. D* 103:023530 (2021)
139. Benevento G, Kable JA, Addison GE, Bennett CL. *Astrophys. J.* 935:156 (2022)
140. Kreisch CD, Cyr-Racine FY, Doré O. *Phys. Rev. D* 101:123505 (2020)
141. Blinov N, Kelly KJ, Krnjaic GZ, McDermott SD. *Phys. Rev. Lett.* 123:191102 (2019)
142. Jedamzik K, Pogosian L. *Phys. Rev. Lett.* 125:181302 (2020)
143. Poulin V, Smith TL, Karwal T, Kamionkowski M. *Phys. Rev. Lett.* 122:221301 (2019)
144. Ivanov MM, et al. *Phys. Rev. D* 102:103502 (2020)
145. Hill JC, McDonough E, Toomey MW, Alexander S. *Phys. Rev. D* 102:043507 (2020)
146. D'Amico G, Senatore L, Zhang P, Zheng H. *J. Cosmol. Astropart. Phys.* 2105:072 (2021)
147. Smith TL, et al. *Phys. Rev. D* 103:123542 (2021)
148. Herold L, Ferreira EGM. arXiv:2210.16296 [astro-ph.CO] (2022)
149. Hill JC, et al. *Phys. Rev. D* 105:123536 (2022)
150. Poulin V, Smith TL, Bartlett A. *Phys. Rev. D* 104:123550 (2021)
151. Wu J, et al. arXiv:2211.06354 [astro-ph.CO] (2022)

Annual Review of Nuclear and Particle Science
Volume 73, 2023

Contents

Errata

An online log of corrections to *Annual Review of Nuclear and Particle Science* articles may be found at http://www.annualreviews.org/errata/nucl